Photophysics of a Butadiyne-Linked Porphyrin Dimer: Influence of Conformational Flexibility in the Ground and First Singlet Excited State

ARTICLE *in* THE JOURNAL OF PHYSICAL CHEMISTRY C · MAY 2007

Impact Factor: 4.77 · DOI: 10.1021/jp0683519

Photophysics of a Butadiyne-Linked Porphyrin Dimer: Influence of Conformational Flexibility in the Ground and First Singlet Excited State

Mikael U. Winters,[†] Joakim Kärnbratt,[†] Mattias Eng,[†] Craig J. Wilson,[‡] Harry L. Anderson,*[,‡] and Bo Albinsson*[,†]

Department of Chemical and Biological Engineering, Physical Chemistry, Kemivägen 3, SE - 412 96 Göteborg, Sweden, and Department of Chemistry, University of Oxford, Chemistry Research Laboratory, Mansfield Road, Oxford OX1 3TA, United Kingdom

Received: December 5, 2006; In Final Form: March 14, 2007

The photophysics of a butadiyne-linked porphyrin dimer has been investigated by spectroscopy and quantum mechanical calculations. Primarily, the influence of conformation on the ground and first singlet excited states was studied, and two spectroscopically distinct limiting cases were identified. Experiments show that the twisted and planar conformers are separate spectroscopic species that can be selectively excited and have unique absorption and emission spectra. Calculated ground-state spectra compare well with experimental spectra of the two species. A spectrum of the planar conformer was obtained by the addition of a dipyridyl pyrrole ligand, which forms a 1:1 complex with the dimer and thus forces it to stay planar. The absorption spectrum of the twisted conformer could be deduced from the excitation spectrum of its emission. The interpretation of the ground-state spectrum of the free noncomplexed dimer is that it represents an average of a broad distribution of conformations. Calculations support this conclusion by indicating that the barrier for rotation is relatively small in the ground state (0.7 kcal/mol). Studies of the temperature dependence of the fluorescence spectrum of the dimer indicate a mother−daughter relationship between the twisted and planar conformations in the excited state, where the former has approximately 3.9 kcal/mol higher energy. Furthermore, time-correlated single-photon counting experiments also suggest that the twisted population adopts a planar configuration in the first singlet excited state with a rate constant of $k_{rot} = 8.8 \times 10^9\ s^{-1}$ in 2-MTHF at room temperature. The temperature dependence of the fluorescence lifetimes indicated that an activation energy barrier of approximately 2 kcal/mol, in part related to solvent viscosity, is associated with this rate constant.

Introduction

Porphyrin oligomers show much promise in many areas of molecular engineering and have been suggested as building blocks for many diverse applications such as artificial photosynthesis,[1] novel optical materials,[2−6] and molecular-scale electronics.[7] Metalloporphyrin oligomers such as zinc(II) complexes are especially versatile, as coordination of ligands such as pyridine and imidazole to the zinc atom facilitates the self-assembly of supramolecular structures, such as boxes and grids.[8−12] The resulting structures can be utilized by addressing individual parts, for instance, by photoexcitation. Various porphyrin oligomers have also been accommodated into donor−acceptor systems to control charge separation,[13−17] particularly with artificial photosynthesis and solar cell applications in mind. Conjugated porphyrin oligomers are attractive from many perspectives, because of their unique electronic properties.[1,7,18] For instance, some butadiyne-linked porphyrin oligomers exhibit large two-photon cross sections[19,20] and hyperpolarizabilities,[2,3] making them interesting candidates for photodynamic therapy and nonlinear refraction. Other potential uses are in the field of molecular electronics, where conjugated porphyrin oligomers are candidate molecular wires.[7,21,22]

The conformation of butadiyne-linked porphyrin oligomers is critical for electronic coupling between the porphyrin macrocycles and, thus, for interporphyrin conjugation. The coupling between porphyrin molecules is strongest when they are coplanar and gradually decreases to a minimum when the units are perpendicular. However, the triple bond potentially allows free rotation, and in principle, a continuous distribution of dihedral angles between adjacent porphyrins is possible for alkyne-linked porphyrin oligomers. It is thus interesting to consider the extent to which this distribution is biased toward the planar conformation, as there is, on one hand, the potential for rotational freedom but, on the other hand, a significant gain in energy to be made from obtaining maximum conjugation. Calculations performed by Stranger et al. on a butadiyne-linked porphyrin dimer indicated essentially barrierless rotation between the dihedral angles 0° and 60° but also pointed to the existence of a significant barrier for rotation above 60°.[23] At 90°, the total energy of the system had increased by approximately 14 kcal/mol relative to that at 0°, indicating that free rotation was not possible at ambient temperature. Therien and co-workers found interesting photophysical properties when describing the ultrafast dynamics of ethyne-linked porphyrin oligomers.[24] In their work, a 30−35-ps component associated with a red shift of the transient signal was found for a meso−meso-linked dimer, and it was hypothesized that this spectral evolution was due to a planarization of nonplanar conformers in the excited state. When time-resolved and steady-state measurements were compared, it was concluded that, although nonplanar conformers were present, the population of maximally conjugated structures was

* To whom correspondence should be addressed. E-mail: balb@chalmers.se (B.A.), harry.anderson@chem.ox.ac.uk (H.L.A.).
[†] Chalmers University of Technology.
[‡] University of Oxford.

10.1021/jp0683519 CCC: $37.00
Published on Web 04/26/2007

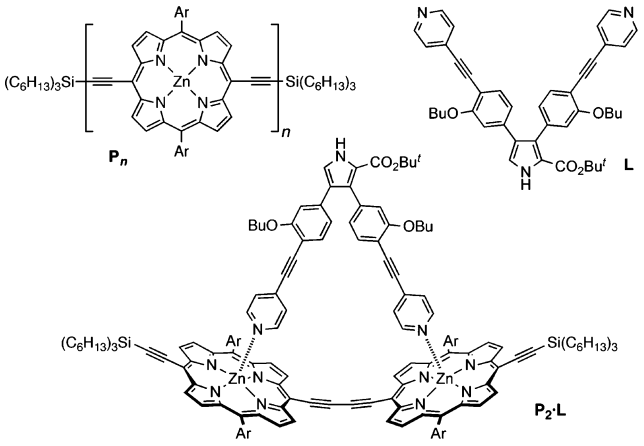

Figure 1. Porphyrin oligomers studied in this work (P_n, $n = 1, 2, 4, 8$) and the dipyridyl pyrrole ligand[26] **L** used to force the dimer into a planar conformation in the $\mathbf{P_2}$·**L** complex. The aryl substituents, Ar, are 3,5-di(octyloxy)phenyl. The bent structure corresponds to a geometry optimized at the PM3 level.

dominant. The group of Aida investigated butadiyne-linked porphyrin dimers with *meso*-pyridyl functionalities that allowed them to form tetrameric boxes. When the resulting structures were characterized spectroscopically, it was found that, surprisingly, the boxes built of perpendicular conformers were favored over the ones built of planar conformers.[25] Apparently, in this configuration, the dipole moments of the pyridyl groups cancelled each other, and the net gain that this provided was enough to overcome any barrier that might have existed. For an ethyne-linked dimer, the boxes were formed exclusively by planar conformers.[11] This result seems to indicate that the barrier for rotation in butadiyne-linked dimers is small.

The issue of conformational heterogeneity is thus an interesting one. The butadiyne-linked zinc porphyrin oligomers ($\mathbf{P}_n$) presented in Figure 1 have previously been incorporated into donor−bridge−acceptor systems ($n = 1, 2, 4$), and their merit as "molecular wires" was studied.[22] In that work, the oligomers served as the electron-mediating structure, and the question of the impact of conformational heterogeneity, in the ground state as well as in the first singlet excited state, is critical, particularly for longer oligomers. Kim, Osuka, and co-workers explored the effects on energy transfer that arise from conformational flexibility in extended, directly linked porphyrin oligomers (up to 512 units)[27] and drew the conclusion that conformational heterogeneities can rule out the use of such structures as energy mediators over long distances. The present work explores the impact of the conformational dynamics described above on the photophysical properties of the simplest member of the oligomer series that exhibits dihedral conformers, the porphyrin dimer in Figure 1 ($n = 2$), and, in particular, the coupling and decoupling of the porphyrin units that occurs during rotation. The basic spectroscopic properties have been described in previous publications[8] and are qualitatively explained by Kasha's point-dipole model for exciton coupling.[28]

Results

Ground-State Absorption. The ground-state absorption spectra of $\mathbf{P}_n$ ($n = 1, 2, 4, 8$) are shown in Figure 2. As a consequence of the stabilization of their excited states by the larger π systems, the B and Q bands of the longer oligomers are red-shifted relative to those of $\mathbf{P}_1$. The interaction between the porphyrin macrocycles results in a splitting of the absorption peaks, which is most clear for $\mathbf{P}_2$ but is largely concealed for $\mathbf{P}_4$ and $\mathbf{P}_8$. For $\mathbf{P}_4$, the spectrum is still structured, and the Q band is formed by several overlapping peaks. The spectral evolution of conjugated porphyrin oligomers is quite interesting, and the features of their ground-state absorption spectra as well as the impact of conformation on these spectra will be discussed in this article.

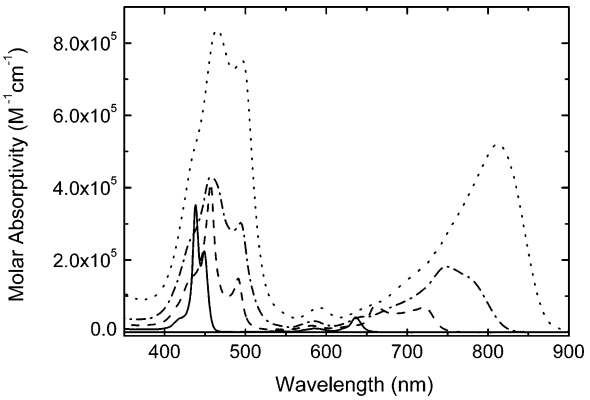

Figure 2. Ground-state absorption spectra of $\mathbf{P}_1$ (solid line, 2-MTHF), $\mathbf{P}_2$ (dashed line, 2-MTHF), $\mathbf{P}_4$ (dash-dotted line, 2-MTHF), and $\mathbf{P}_8$ (dotted line, DCM/pyridine).

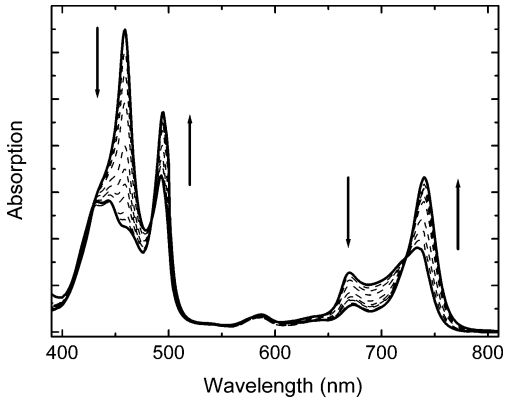

Figure 3. Titration of a solution of $\mathbf{P}_2$ in dichloromethane (approximately 0.8 μM) containing a small quantity of pyridine (0.1 vol %) with the dipyridyl pyrrole ligand **L** (added in excess, $c_{final} \geq 10$ μM) to form the $\mathbf{P_2}$·**L** complex. Isosbestic points are located at 484 and 723 nm.

To test how the absorption spectrum of the porphyrin dimer depends on its conformation (or rather, on its distribution of conformations), a concentrated solution of the bidentate dipyridyl pyrrole ligand L (Figure 1) was used to titrate a sample of $\mathbf{P}_2$ dissolved in dichloromethane (Figure 3). A small quantity of pyridine was added before the titration to avoid shifts in the spectrum due to complexation. The dipyridyl pyrrole ligand L forms a strong 1:1 complex with $\mathbf{P}_2$ ($K \approx 10^7-10^8$ mol^{-1} dm^3, Supporting Information) that effectively forces the dimer to stay planar or very nearly planar and was added in sufficient excess so that the competition from pyridine was of no consequence. The intensity of the B band peak at 457 nm decreases upon titration, whereas the intensity of the peak at 491 nm increases. In the Q band, the intensity of the peak farthest to the red increases, and that of the peak on the blue side decreases. The absorption of the ligand itself is in the UV, with a maximum at 340 nm. Thus, the final spectrum above 400 nm is almost exclusively that of the planar dimer, which exhibits two peaks in the B band and one strong peak in the Q band. It is similar to the spectrum of an aggregated dimer,[8] as expected. The bending of the porphyrin dimer upon complexation has minor effects on the absorption spectra, as shown in Figure 3, and this is also supported by quantum mechanical calculations (vide

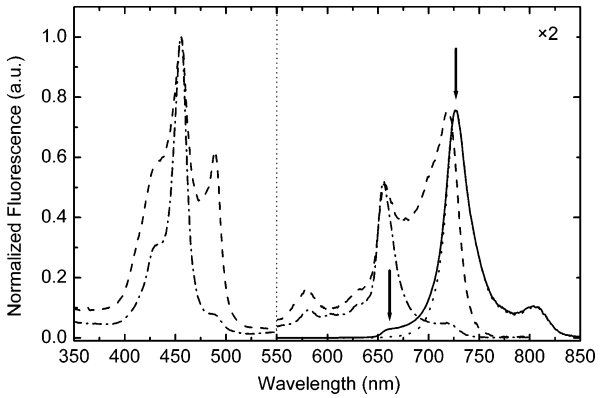

Figure 4. Emission and excitation spectra of $\mathbf{P}_2$ recorded in 2-MTHF. Emission spectra were recorded using the excitation wavelengths 457 nm (solid line) and 491 nm (dotted line). The emission wavelengths (indicated by arrows) used for the excitation spectra were 666 nm (dash-dotted line) and 727 nm (dashed line). The Q band is slightly distorted due to scattering. Note that the excitation spectra in the right panel are scaled by a factor of 2.

infra). In contrast, the ground-state absorption spectrum of disaggregated $\mathbf{P}_2$, free to rotate, is a mixture of several spectroscopic species. UV−vis titrations of $\mathbf{P}_2$ with the dipyridyl pyrrole ligand **L** were also performed in dichloromethane and chloroform in the absence of pyridine (Figures S1 and S2, Supporting Information), and the spectral changes were found to be very similar to those shown in Figure 3.

Fluorescence Spectroscopy. When $\mathbf{P}_2$ was excited at the four main peaks, the fluorescence spectrum of $\mathbf{P}_2$ exhibited a dependence on excitation wavelength (Figure 4). When the dimer was excited at either of the B or Q band peaks of higher energy (457 nm or 661 nm), a weak fluorescence peak was present at 666 nm (indicated by an arrow in Figure 4) that did not appear when the sample was excited at any of the peaks of lower energy (491 or 721 nm). This peak arose irrespective of the solvent used [dichloromethane (DCM)/pyridine, tetrahydrofuran (THF), and 2-methyltetrahydrofuran (2-MTHF) were tested]. Moreover, excitation spectra were recorded for emissions at 666 and 727 nm (Figure 4, dashed curves). Whereas recording the excitation spectra of the emission at 727 nm reproduced a spectrum resembling the full ground-state absorption spectrum, the emission at 666 nm did not reproduce the full spectrum but rather produced a spectrum that exhibits only two of its peaks. This spectrum is much more like that of a porphyrin monomer, albeit shifted to the red. This result indicates that the origin of this emission peak in the steady-state spectrum is due to a distinctive spectroscopic species. As it was established from ground-state absorption that the planar conformation has a unique ground-state absorption spectrum, it thus seems plausible that there is a spectroscopic difference between the planar and twisted conformations of $\mathbf{P}_2$. The excitation spectrum obtained from the emission at 666 nm well mirrors the absorption spectrum of a twisted conformation.

The emission at 666 nm was further investigated by measuring the steady-state spectrum at lower temperatures. For excitation at 457 or 661 nm, a strong temperature dependence was found, as demonstrated in Figure 5. At room temperature, the strongest emission is at 727 nm, whereas the peak at 666 nm is only a small shoulder on the blue side of the main peak. As the temperature is lowered, the main emission is gradually weakened, and the intensity of the emission at 666 nm grows strongly. This seems to exclude the possibility that the low emission shoulder is due to an impurity, but rather indicates that the two emitting species stand in a mother−daughter

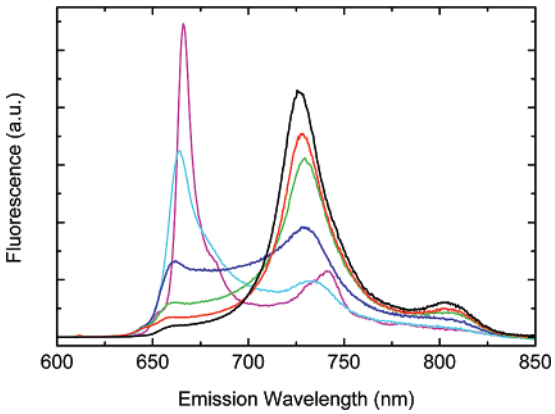

Figure 5. Steady-state fluorescence spectra of $\mathbf{P}_2$ recorded in 2-MTHF at 295 K (black), 255 K (red), 215 K (green), 175 K (blue), 135 K (cyan), and 95 K (magenta). The sample was excited at 457 nm.

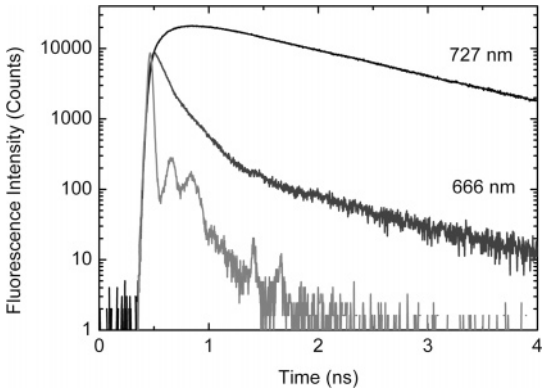

Figure 6. Fluorescence decay traces for $\mathbf{P}_2$ in 2-MTHF at 295 K. The sample was excited at 457 nm, and the emission was monitored at 666 nm (dark gray trace) and 727 nm (black trace). The instrument response function is represented by the light gray trace. Note that the scale of the abscissa is logarithmic.

relation to one another that is strongly temperature-dependent. This suggests that the population of twisted conformers, which were assigned to the emission at 666 nm, adopt a planar configuration in the excited state. When the corresponding measurements were made by exciting at 491 nm, no large temperature effects were observed in the fluorescence spectrum.

To further test the idea that the twisted and planar conformations are separate spectroscopic species with unique absorption and emission spectra, time-correlated single-photon counting (TCSPC) was used to measure the fluorescence lifetimes of the porphyrin dimer at the two emission peaks. The temperature dependence of the fluorescence lifetimes at these wavelengths was then studied. The fluorescence lifetime decay was recorded at 5-nm intervals over the entire emission spectrum at room temperature to visualize the spectral evolution. It was found that, shortly after excitation at 457 nm, the spectrum resembled that found by steady-state fluorescence measurements at 95 K, but after approximately 500 ps, the spectrum had evolved into that found at 295 K (Figure S3, Supporting Information). Moreover, when the sample was excited at 457 nm, two fluorescence lifetimes were necessary to fit the resulting fluorescence decay curves (Figure 6). The fluorescence at 666 nm was dominated by a fast decay, whereas the fluorescence at 727 nm exhibited a corresponding rise time in the emission and a subsequent slow decay (Table 1). This again suggests that the species emitting at short and long wavelengths stand in a mother−daughter relationship. At both emission wavelengths, the long lifetime was approximately 1.2 ns at room

TABLE 1: Temperature Dependence of the Fluorescence Lifetimes for P_2 in 2-MTHF, Excited at 457 nm

	emission wavelength = 666 nm				emission wavelength = 727 nm				
T (K)	τ_1 (ps)	$\alpha_1{}^{a,b}$	$f_1{}^{a,b}$ (%)	χ^2	τ_1 (ps)	$\alpha_1{}^{a}$	τ_2 (ns)	$\alpha_2{}^{a}$	χ^2
295	100	0.96	80	2.8[c]	120	−0.47	1.21	0.53	1.6
255	160	0.97	90	2.4[c]	300	−0.48	1.27	0.52	1.6
215	290	1	100	1.7	340	−0.43	1.33	0.57	2.0
175	480	1	100	1.5	720	−0.32	1.35	0.68	1.6
135	730	0.82	77	1.4	850	0.16	1.38	0.84	1.5
95	820	0.99	97	1.4	–	–	1.44	1	1.3

[a] α is the normalized preexponential factor, and f_1 is the fractional fluorescence intensity [b] Because of a small spectral overlap, a fraction of the longer emission lifetime is also present at this wavelength. [c] Measurements in a cryostat lead to higher χ^2 values than normal. See Experimental Section.

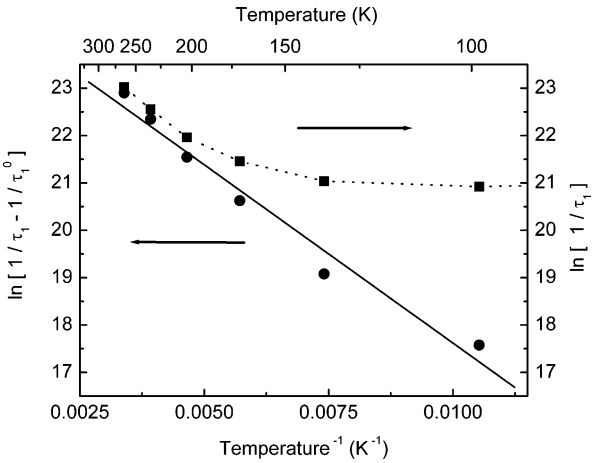

Figure 7. Temperature dependence of the fluorescence lifetime data of $\mathbf{P}_2$ in 2-MTHF, plotted as $\ln(1/\tau_1)$ (squares) and $\ln(1/\tau_1 - 1/\tau_1{}^0)$ (circles); see Table 1. The straight solid line is a linear regression to the $\ln(1/\tau_1 - 1/\tau_1{}^0)$ data, yielding $E_a = 2$ kcal/mol.

temperature. When the sample was excited at either 491 or 721 nm, the fluorescence decay was monoexponential and exhibited no emission at 666 nm. As the temperature was lowered, it was found that both the short fluorescence decay and the corresponding rise time became progressively longer, whereas the longer decay lifetime was not much affected (Table 1). This shows that the process connecting the two excited states is sensitive to temperature, making a rotation around the butadiyne axis a plausible explanation, and that the planar conformation is preferred in the first excited singlet state.

Furthermore, it appears that this rotation is almost completely hindered at 95 K (Figure 7), and therefore, it was assumed that the fluorescence lifetime measured at 666 nm is approximately equal to the intrinsic fluorescence lifetime of the twisted conformation ($\tau_1{}^0$). The rate constant for rotation was calculated as $k_{rot} = [1/\tau_1 - 1/\tau_1{}^0]$, and in Figure 7, $\ln(k_{rot})$ is presented together with $\ln(1/\tau_1)$. By using the Arrhenius equation, an apparent activation energy of 2 kcal/mol was obtained by linear regression of $\ln(k_{rot})$, indicating the possibility of an activation energy for rotation in the excited state. To clarify the extent to which the determined activation energy is related to solvent viscosity effects, the temperature dependence of the viscosity of 2-MTHF was checked. The Andrade equation, $\eta(T) = A_\eta \exp(E_\eta/RT)$, can be used to check the viscous contribution to the rotational barrier, and this was done for 2-MTHF using data from ref 29, which yielded $E_\eta \approx 2$ kcal/mol for the linear region. As 2-MTHF is a glass-forming solvent, its viscosity exhibits a very strong temperature dependence at low temperatures, and thus, the Andrade equation applies only down to moderately low temperatures for this solvent. Young et al. used the Williams−Landel−Ferry equation, $\eta(T) = A_\eta \exp[E_\eta/R(T - T_0)]$, for 2-MTHF (characteristic temperature $T_0 = 81$ K) and obtained a viscous barrier of $E_\eta = 0.74$ kcal/mol.[29] This also suggests that a significant part of the activation energy is due to viscous effects, but as this equation is more appropriate for glass-forming solvents, the estimated contribution of viscosity to E_a is probably more accurate.

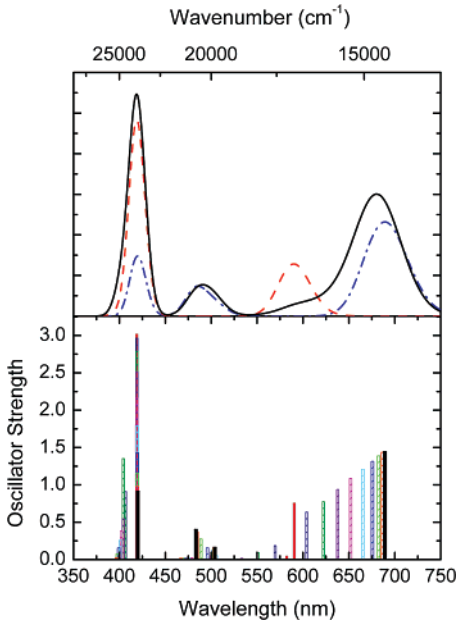

Figure 8. (Bottom) Calculated ground-state stick spectra at different dihedral angles: 0° (black, solid) and 90° (red, solid) represent the border cases and the intermediate dihedral angles are represented by hatched bars [10° (red), 20° (green), 30° (royal blue), 40° (cyan), 50° (magenta), 60° (violet), 70° (dark green), 80° (navy blue)]. (Top) Calculated spectra fitted to Gaussian components with half-widths at half-maximum arbitrarily set to 1000 cm^{-1}: 0° (blue, dot-dashed line), 90° (red, dashed line), and a simulated room-temperature spectrum (black, solid line) based on a Boltzmann-weighted combination of the 10 (0−90°) conformers using the calculated ground-state potential energy surface (Figure 9).

Quantum Mechanical Calculations. Calculated electronic transitions of 10 different conformations of $\mathbf{P}_2$ are shown in Figure 8. It is evident from these results that increasing the dihedral angle from 0° to 90° results in a blue shift of the Q band and an intensified B band transition at 420 nm. At a dihedral angle of 0°, the B band consists of two strong transitions, and the Q band consists of only one. This is in qualitative agreement with the spectrum of the planar conformation displayed in Figure 3. At a dihedral angle of 90°, a blue-shifted Q band is present, and only one major transition in the B band remains. This, in turn, reproduces the excitation spectrum in Figure 4 that is believed to resemble the absorption spectrum of the twisted conformation. The bending of $\mathbf{P}_2$ that is induced by the addition of the ligand **L** results in a small red shift of the transitions, but the effect is minor compared to that of twisting.

The tendency to form the planar conformation in the excited state can be understood by comparing the potential energy surfaces of the S_0 and S_1 states. In Figure 9, the potential energy is plotted as a function of the torsion angle. The ground-state energies were obtained by full geometry optimization of $\mathbf{P}_2$ at several torsion angles between 0° and 90°, whereas the excitation energies of the planar and twisted conformers were taken from

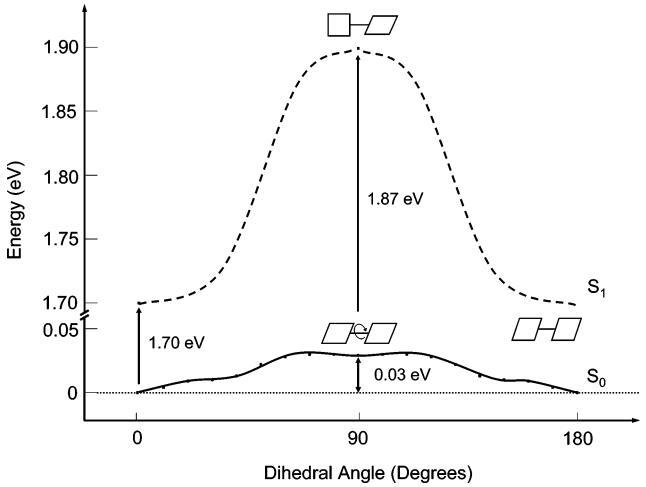

Figure 9. S_0 and S_1 potential energy surfaces of $\mathbf{P}_2$. The S_0 surface was calculated at the BLYP/6-31G(d) level. The E_{00} values for the twisted and planar conformation were determined from spectra, and the dashed black line indicates an approximate PES for S_1. The calculated ground-state barrier for rotation (0.67 kcal/mol) is indicated by a double-headed arrow.

absorption and emission spectra of $\mathbf{P}_2$. The calculations indicate that the ground state exhibits a very low barrier for rotation (0.67 kcal/mol) and should thus have a broad distribution of dihedral angles at room temperature. Nevertheless, the ground-state absorption spectrum of $\mathbf{P}_2$ is quite structured, as is evident in Figure 2, and this is also supported by the calculated transitions (vide infra). The value found for the barrier to rotation is similar to the estimated 1 kcal/mol obtained by Lin et al. from AM1 semiempirical calculations on a similar porphyrin dimer[30] and also similar to experimental values reported for diphenylethyne- and diphenylbutadiyne-linked porphyrins (0.79 and $<$0.79 kcal/mol, respectively).[31] For a porphyrin dimer related to ours, Stranger et al. reported a potential energy surface that exhibits an energy difference between the planar and perpendicular conformations of more than 15 kcal/mol.[23] It is unlikely, however, that interporphyrin conjugation should represent a stabilization of the planar conformer amounting to such a high energy. On the contrary, we believe that the ground-state absorption spectrum indicates that a significant fraction of molecules populate dihedral angles near 90° at room temperature. In the excited state, the energy difference between the twisted and planar conformers is approximately 3.9 kcal/mol (0.17 eV/molecule), so that planarization of the twisted conformer yields a considerably larger energy gain in the excited state than in the ground state and the rotation is thus constrained, which explains the strong bias toward the planar conformer of $\mathbf{P}_2$ in the excited state.

Discussion

The present study is concerned with the effects of the conformational dynamics of a butadiyne-linked porphyrin dimer and has identified two spectroscopically distinct limiting cases, which have been assigned to a twisted conformation and a planar conformation. The continuous distribution of states from twisted to planar is described well by the calculations presented above (Figure 8). Spectroscopically, however, the system behaves like a two-state system, which means that we can prepare the molecule in either a planar or a twisted excited state by selecting the appropriate excitation wavelength (Figure 4). If the porphyrin dimer is in solution and is free to rotate, the ground-state absorption spectrum is an average spectrum of the absorptions of all possible conformations from planar to perpendicular, because of the low-energy barrier to rotation. Figures 3 and 4 basically show spectra of the individual species and demonstrate that, if a sample is excited at 491 or 721 nm, the planar conformation is exclusively excited, whereas if a sample is excited at 661 nm, only the twisted conformation is excited. At 457 nm, both conformations absorb, but the transition of highest intensity belongs to the twisted conformation. This makes it possible to learn about the conformational dynamics of this system with simple means, i.e., by studying how the system evolves after excitation.

Further support for the interpretation of the absorption spectrum of $\mathbf{P}_2$ comes from quantum mechanical calculations. In short, both the split Q and B bands are explained by the calculations: The planar form has a single electronic transition at 690 nm and a split B band with transitions at 420 and 490 nm, whereas the twisted, 90° structure has two isolated electronic transitions calculated at 420 and 590 nm (Figure 8). The lowest electronic transition, corresponding to the Q band, gradually blue shifts (690 → 590 nm) and weakens slightly as the dihedral angle increases. In contrast, the high-energy component of the B band (calculated at 420 nm) increases in intensity without changing its calculated wavelength. The low-energy component observed for the planar form disappears as the dihedral angle approaches 90°. The assignment of the observed absorption and excitation spectra are, thus, strongly supported by the qualitative interpretation of the calculations; The lowest-energy components of both the Q and B bands are due to the planar form, and the high-energy components are due to the twisted form (the high-energy B band also has contributions from the planar form). In view of the shallow calculated ground-state potential surface, it might initially seem surprising that the absorption and excitation spectra are structured with features identifiable with the planar and twisted conformers. However, as a consequence of the variation of the transition moments (energies and intensities) with the dihedral angle, the spectra display bands associated with these limiting conformations and, therefore, appear to be composed of only two components even though the molecule has a broad distribution of dihedral angles.[23,32] The underlying reason for this unexpected observation is discussed in terms of orbital and state correlations in the next paragraph.

The molecular structure of $\mathbf{P}_2$ approximately belongs to the D_2 point group with three mutually perpendicular C_2 axes. The planar and perpendicular conformers have additional symmetry elements raising the symmetries to D_{2h} and D_{2d}, respectively. In the D_2 point group, the π orbitals transform as the irreducible representations a, b_1, b_2, and b_3 (i.e., all available species in this point group), and these correlate with the a_u, b_{1g}, b_{2g} and b_{3u} species in the D_{2h} point group. In Figure 10, the calculated orbital energies for the four highest occupied and four lowest unoccupied orbitals are shown as a function of the dihedral angle.[32−34] It is quite obvious that the a and b_1 orbital energies do not depend on the angle between the porphyrin planes whereas the b_2 and b_3 orbitals depend strongly on this angle. This is easy to understand, given that the a and b_1 π orbitals are symmetric with respect to rotation about the z axis (long axis along the butadiyne linker) so that it is not possible for these orbitals to spread over the butadiyne linker, which makes them localized on the porphyrin fragments. The b_2 and b_3 orbitals, however, are antisymmetric with respect to z-axis rotation, so that they delocalize over the butadiyne linker and couple the porphyrin fragments strongly; as an inevitable consequence, their energies show a strong dihedral angle

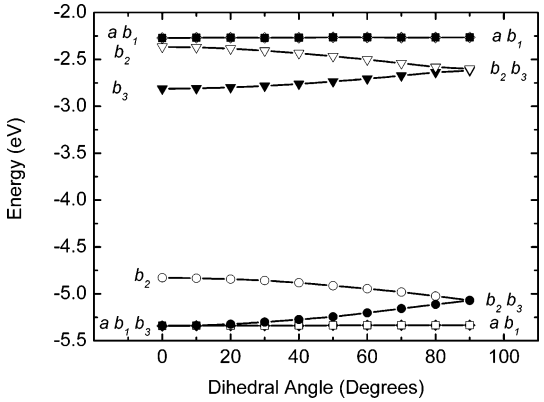

Figure 10. Calculated orbital energies for the four highest occupied and the four lowest unoccupied orbitals as a function of the dihedral angle (HOMO − 3 is represented by solid diamonds, HOMO − 2 by open squares, HOMO − 1 by solid circles, HOMO by open circles, LUMO by solid triangles, LUMO + 1 by open triangles, LUMO + 2 by solid squares, and LUMO + 3 by open diamonds). The orbital symmetries from HOMO − 3 to LUMO + 3 are a, b_1, b_3, b_2, b_3, b_2, a, and b_1, respectively. See Supporting Information for graphical representations of the molecular orbitals (Figure S3).

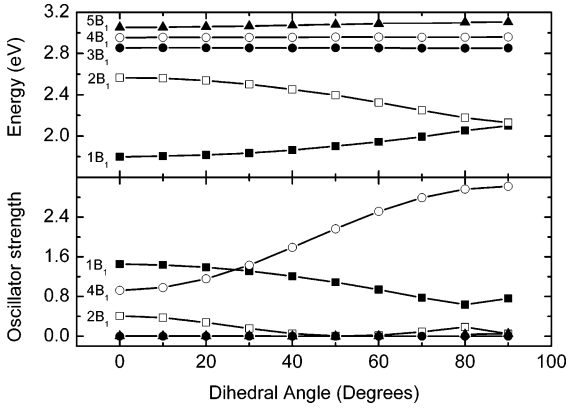

Figure 11. State correlation diagram of the calculated states of B_1 symmetry as a function of the dihedral angle. $1B_1$ is represented by solid squares, $2B_1$ by open squares, $3B_1$ by solid circles, $4B_1$ by open circles, and $5B_1$ by solid triangles.

dependence. Both the occupied and unoccupied a and b_1 orbitals in Figure 10 are accidentally (almost) degenerate for all dihedral angles. We can carry this quite general symmetry analysis further by noting that the b_2 and b_3 orbitals are symmetric and antisymmetric, respectively, with respect to rotation about the *y* axis (short in-plane axis for the planar configuration) and vice versa for the *x* axis (short out-of-plane axis). This means that the π orbitals belonging to the b_2 species are "antibonding" over the butadiyne bridge and the b_3 orbitals are "bonding". As expected, the energy of the b_2 orbitals decreases as the dihedral angle increases, whereas the b_3 energies increase as they lose their π overlap upon twisting. To correlate these changes in molecular orbital energies with spectral observations, one needs to consider the possible electronic excited states that can be formed and which of those have strong, electric-dipole-allowed transitions with the ground state (of symmetry A_1).

In the present calculation, transitions to excited states belonging to the irreducible representation B_1 are strong and long-axis-polarized, whereas symmetry-allowed transitions to the other states of B_2 and B_3 symmetries are generally weak. This conclusion is supported by previous reports in the literature, in which the majority of the strong transitions observed in the absorption spectrum of $\mathbf{P}_2$ were shown to be long-axis-polarized.[35] For this reason, only the states of B_1 symmetry are considered here. A correlation diagram of the B_1 states is shown in Figure 11. The excited states of B_1 symmetry are composed of singly excited configurations in which an electron in either the a or b_1 orbitals is promoted to the b_1 or a orbitals, respectively, and/or an electron in the b_2 or b_3 orbitals is promoted to the b_3 or b_2 orbitals, respectively. These electronic configurations can all contribute to the final-state wavefunction of B_1 symmetry. Now, considering only the four highest occupied and four lowest unoccupied orbitals (see Figure 10), the following single-electron substitutions of B_1 symmetry are possible (approximately in increasing energy order): $b_2 \rightarrow b_3$, $b_3 \rightarrow b_2$, a $\rightarrow$ b_1, and $b_1 \rightarrow$ a. The lowest electronic transition, corresponding to the Q band, has B_1 symmetry ($1B_1$) and is dominated by the $b_2 \rightarrow b_3$ (HOMO $\rightarrow$ LUMO) excitation for all dihedral angles except 90°. This transition shifts to higher energy and loses some intensity, as seen in the state correlation diagram (Figure 11), which could easily be understood in terms of the orbital shifts displayed in Figure 10. The difference in rotational barrier for the S_0 and S_1 states (Figure 9) could also be traced back to the destabilization of the LUMO (b_3) orbital upon twisting. The next B_1 transition, calculated at 483 nm for the planar conformation, is part of the B band, but it shifts to lower energy and loses intensity as the dihedral angle increases. At 90°, the two lowest B_1 transitions almost coincide to form a pair of transitions that is expected to absorb at 590 nm (the Q band of the twisted conformer). This $2B_1$ transition is dominated by the $b_3 \rightarrow b_2$ (HOMO − 1 $\rightarrow$ LUMO + 1) configuration, and its red shift is understood in terms of the decreased orbital splitting in Figure 10.

Finally, the strong transition to the $4B_1$ state, corresponding to the high-energy component of the B band, has an excitation energy that is almost independent of the dihedral angle. The distribution of electron configurations contributing to this transition is quite broad at all dihedral angles, but it is dominated by the a $\rightarrow$ b_1 and $b_1 \rightarrow$ a configurations, at least at large dihedral angles. Apparently, the configurations contributing to this transition either have no dependence of the dihedral angle (a $\rightarrow$ b_1 and $b_1 \rightarrow$ a) or occur as a balanced mixture of configurations that increase ($b_2 \rightarrow b_3$) and decrease ($b_3 \rightarrow b_2$) in energy. Transitions to the $3B_1$ and $5B_1$ states included in Figure 10 have very small transition moments and are therefore not considered here.

The first singlet excited state of the twisted conformer has higher energy than the first excited state of the planar conformer, which is apparent from experiments and has also been confirmed by calculations. The fluorescence studies performed show that both states emit and that their fluorescence spectra are unique. At room temperature, the emission maximum of the twisted conformation is 666 nm, whereas that of the planar conformation is 727 nm. When the twisted conformation was selectively excited and the fluorescence lifetimes were measured at the emission maxima of the twisted and planar conformations, it was found that the fluorescence decay of the twisted state agreed with the rise time found for the planar conformation, indicating that the excited state of this system relaxes to a planar conformation. This confirms the hypothesis put forth by Therien and co-workers.[24] In their work, an evolution in transient spectra on the 30−35-ps time scale was found for a meso−meso ethyne-linked dimer that was believed related to a dynamical relaxation of the nonplanar population. It was further hypothesized that there should be a small energy barrier to rotation from the perpendicular conformation in the excited state. The evolution of the nonplanar excited population into a planar configuration has been confirmed by this work, and the existence of a small

activation energy barrier, probably partially related to solvent viscosity, has been demonstrated by the temperature dependence of the fluorescence lifetimes.

Conclusions

To conclude, the results presented in this work strongly suggest that butadiyne-linked porphyrin dimers in the ground state are free to explore all dihedral angles between 0° and 90° with only a small energy cost. This was demonstrated both by experiment and by quantum mechanical calculations. Moreover, all important spectral features of the ground-state absorption spectrum can be explained on the basis of this conclusion. At room temperature, the heterogeneity found in the ground state is replaced by a more or less uniform planar conformation in the first singlet excited state, as shown by fluorescence studies. It is interesting to generalize these findings to longer oligomers, such as $\mathbf{P}_4$ and $\mathbf{P}_8$ (Figure 2). It is shown in this work that, if the dimer is excited sufficiently far to the red side of the Q band, only planar conformers absorb. Moreover, exciting on the blue side exclusively excites the population of twisted conformers. This finding should hold equally well for $\mathbf{P}_4$ and $\mathbf{P}_8$, which means that the shape of the Q band will be determined by the statistical distribution of conformations weighted by their respective Boltzmann factors. That is, as the chain grows longer, the relative weight of the conformations having either all porphyrin macrocycles coplanar or all porphyrin macrocycles mutually perpendicular will decrease. This result is suggested by the spectra of $\mathbf{P}_4$ and $\mathbf{P}_8$ in Figure 2. In the Q bands of these oligomers, a large number of conformers with dihedral angles ranging from 0° to 90° contribute. It is expected that each of these conformers has only one strong, long-axis-polarized transition in this region with a transition energy strongly dependent on the dihedral angles but an oscillator strength that varies only slightly. Because the statistical weight of conformers with combinations of dihedral angles deviating from 0° or 90° grows as the oligomer length increases, the Q band develops a more Gaussian band shape. Thus, two simple predictions can be made for the longer chains: First, the choice of excitation wavelength is critical for initial preparation of the excited state of conjugated porphyrin oligomers of this kind, and second, a strong temperature dependence of the absorption and fluorescence spectra is expected, particularly for the longer chains. We plan to investigate both of these predictions in the near future.

For future studies of electron or energy transfer using conjugated porphyrin oligomers of the kind presented in Figure 1, the demonstrated conformational heterogeneity is of fundamental importance, as it might impede mediation of electrons or energy, particularly in longer systems.[27,36] In a previous work, the tunneling barrier for electron transfer through porphyrin oligomers up to $n = 4$ was believed to stem primarily from barriers at the junctions to the electron donor and an acceptor moieties.[22] The rate of electron transfer might, however, also be affected by conformational heterogeneity, as it is easy to imagine that certain permutations could affect the electron-transfer properties by decreased electronic coupling or by the creation of electron "traps". Restraining the possible distribution of conformers, e.g., by complexation to ligands such as that presented in Figure 1, is a practical way of studying these effects, and such work is now in progress.[42]

Experimental Section

Materials. The solvents used for this study were dichloromethane (DCM, Acros), tetrahydrofuran (THF, Acros), and 2-methyltetrahydrofuran (2-MTHF, Acros). The solvents were always freshly distilled before use.

Spectroscopy. Absorption spectra were measured on a Cary 4B UV−vis spectrophotometer. The spectra were recorded between 300 and 850 nm at 300 nm/min with a spectral bandwidth of 0.5 nm. The sample was contained in a 10-mm quartz cuvette, and a new baseline was recorded for each sample. Fully corrected emission and excitation spectra were recorded on a Spex Fluorolog 3 instrument equipped with a xenon lamp. To avoid aggregation and inner-filter effects, the concentrations of the samples were low, approximately 0.1−1 μM in most cases. The spectral bandwidth for the emission and excitation monochromators was between 1 and 4 nm and was chosen to obtain a good signal-to-noise ratio. Time-resolved fluorescence measurements were performed by time-correlated single-photon counting. The excitation pulse was provided by a Tsunami Ti: sapphire laser (Spectra-Physics) that was pumped by a Millennia Pro X laser (Spectra-Physics). The Tsunami output was tuned to either 920 or 990 nm and subsequently frequency-doubled to 460 or 495 nm. The emission photons were collected by a thermoelectrically cooled microchannel plate photomultiplier tube (R3809U-50, Hamamatsu). The signal was digitalized using a multichannel analyzer with 4096 channels (SPC-300, Edinburgh Analytical Instruments), and to get good statistics, at least 10 000 counts (top channel) were recorded for each decay. The fluorescence decay curves were fitted to two-exponential expressions with the program FluoFit Pro v.4 (PicoQuant GmbH), both individually and with global parameters.

Temperature Studies. For the temperature-dependent absorption and emission studies, a temperature-controlled liquid nitrogen cryostat (Oxford Instruments) was used. The samples were degassed by repeated freeze−pump−thaw cycles prior to measurements to exclude any effects due to quenching reactions caused by oxygen. Using a cryostat for TCSPC measurements introduced difficulties when the fluorescence lifetimes were short, because the instrument response function contains more scattered light in this case. χ^2 thus become larger than normal. In particular, this is a problem when the emission intensity is weak. The results were controlled by comparison with measurements in a regular cuvette at room temperature, when possible.

Quantum Mechanical Calculations. The Gaussian 03 program suite[37] was used to calculate optimized geometries and electronic transitions for a model compound similar to $\mathbf{P}_2$ with the aryl side groups replaced by phenyl groups and the trihexylsilyl groups replaced by hydrogen atoms. These substitutions significantly decrease the calculation time but are still believed to conserve the π system of $\mathbf{P}_2$. Ten different conformations of the model compound with torsion angles ranging from 0 to 90° were constructed and optimized for all other parameters using the B3LYP functional[38−40] and the 6-31G(d) basis set.[41] Time-dependent density functional theory (TD−DFT) was then applied to the optimized structures to evaluate the ground-state electronic spectrum of $\mathbf{P}_2$ as a function of torsion angle. Both the geometry optimizations and the TD−DFT-calculations were all constrained to the D_2 symmetry of the porphyrin dimer. Test calculations without symmetry constraints resulted in no significant difference in either the final geometry or the calculated spectrum. Bond lengths in the central butadiyne unit were estimated to be 1.416 Å (*meso*-C−C), 1.225 Å (C≡C), and 1.355 Å (central C−C) and compared well with values obtained from a reported crystal structure: 1.429 Å (*meso*-C−C), 1.210 Å (C≡C), and 1.369 Å (central C−C).[18]

Acknowledgment. This work was funded by the Swedish Research Council (VR), the Knut and Alice Wallenberg Foundation, and the EPSRC.

Supporting Information Available: UV−vis titrations in DCM and chloroform, time evolution of the $\mathbf{P}_2$ fluorescence spectrum, and molecular orbital representations. This material is available free of charge via the Internet at http://pubs.acs.org.

References and Notes

(1) Lin, V. S. Y.; DiMagno, S. G.; Therien, M. J. *Science* **1994**, *264*, 1105−1111.

(2) Anderson, H. L.; Martin, S. J.; Bradley, D. D. C. *Angew. Chem., Int. Ed. Engl.* **1994**, *33*, 655−657.

(3) Beljonne, D.; O'Keefe, G. E.; Hamer, P. J.; Friend, R. H.; Anderson, H. L.; Bredas, J. L. *J. Chem. Phys.* **1997**, *106*, 9439−9460.

(4) Kuebler, S. M.; Denning, R. G.; Anderson, H. L. *J. Am. Chem. Soc.* **2000**, *122*, 339−347.

(5) Priyadarshy, S.; Therien, M. J.; Beratan, D. N. *J. Am. Chem. Soc.* **1996**, *118*, 1504−1510.

(6) LeCours, S. M.; Guan, H. W.; DiMagno, S. G.; Wang, C. H.; Therien, M. J. *J. Am. Chem. Soc.* **1996**, *118*, 1497−1503.

(7) Anderson, H. L. *Chem. Commun.* **1999**, 2323−2330.

(8) Anderson, H. L. *Inorg. Chem.* **1994**, *33*, 972−981.

(9) Wilson, G. S.; Anderson, H. L. *Chem. Commun.* **1999**, 1539−1540.

(10) Hwang, I. W.; Cho, H. S.; Jeong, D. H.; Kim, D.; Tsuda, A.; Nakamura, T.; Osuka, A. *J. Phys. Chem. B* **2003**, *107*, 9977−9988.

(11) Tsuda, A.; Hu, H. F.; Watanabe, R.; Aida, T. *J. Porphyrins Phthalocyanines* **2003**, *7*, 388−393.

(12) Hwang, I. W.; Kamada, T.; Ahn, T. K.; Ko, D. M.; Nakamura, T.; Tsuda, A.; Osuka, A.; Kim, D. *J. Am. Chem. Soc.* **2004**, *126*, 16187−16198.

(13) Imahori, H.; Guldi, D. M.; Tamaki, K.; Yoshida, Y.; Luo, C. P.; Sakata, Y.; Fukuzumi, S. *J. Am. Chem. Soc.* **2001**, *123*, 6617−6628.

(14) Imahori, H.; Tamaki, K.; Guldi, D. M.; Luo, C. P.; Fujitsuka, M.; Ito, O.; Sakata, Y.; Fukuzumi, S. *J. Am. Chem. Soc.* **2001**, *123*, 2607−2617.

(15) Imahori, H.; Tamaki, K.; Araki, Y.; Sekiguchi, Y.; Ito, O.; Sakata, Y.; Fukuzumi, S. *J. Am. Chem. Soc.* **2002**, *124*, 5165−5174.

(16) Imahori, H.; Sekiguchi, Y.; Kashiwagi, Y.; Sato, T.; Araki, Y.; Ito, O.; Yamada, H.; Fukuzumi, S. *Chem. Eur. J.* **2004**, *10*, 3184−3196.

(17) Guldi, D. M.; Imahori, H.; Tamaki, K.; Kashiwagi, Y.; Yamada, H.; Sakata, Y.; Fukuzumi, S. *J. Phys. Chem. A* **2004**, *108*, 541−548.

(18) Taylor, P. N.; Huuskonen, J.; Rumbles, G.; Aplin, R. T.; Williams, E.; Anderson, H. L. *Chem. Commun.* **1998**, 909−910.

(19) Karotki, A.; Drobizhev, M.; Dzenis, Y.; Taylor, P. N.; Anderson, H. L.; Rebane, A. *Phys. Chem. Chem. Phys.* **2004**, *6*, 7−10.

(20) Drobizhev, M.; Stepanenko, Y.; Dzenis, Y.; Karotki, A.; Rebane, A.; Taylor, P. N.; Anderson, H. L. *J. Am. Chem. Soc.* **2004**, *126*, 15352−15353.

(21) Kim, D.; Osuka, A. *Acc. Chem. Res.* **2004**, *37*, 735−745.

(22) Winters, M. U.; Dahlstedt, E.; Blades, H. E.; Wilson, C. J.; Frampton, M. J.; Anderson, H. L.; Albinsson, B. *J. Am. Chem. Soc.* **2007**, *129*, 4291−4297.

(23) Stranger, R.; McGrady, J. E.; Arnold, D. P.; Lane, I.; Heath, G. A. *Inorg. Chem.* **1996**, *35*, 7791−7797.

(24) Kumble, R.; Palese, S.; Lin, V. S. Y.; Therien, M. J.; Hochstrasser, R. M. *J. Am. Chem. Soc.* **1998**, *120*, 11489−11498.

(25) Tsuda, A.; Hu, H. F.; Tanaka, R.; Aida, T. *Angew. Chem., Int. Ed.* **2005**, *44*, 4884−4888.

(26) Hoffman, M.; Wilson, C. J.; Odell, B.; Anderson, H. L. *Angew. Chem., Int. Ed.* **2007**, *46*, 3122−3125.

(27) Ahn, T. K.; Yoon, Z. S.; Hwang, I. W.; Lim, J. K.; Rhee, H.; Joo, T.; Sim, E.; Kim, S. K.; Aratani, N.; Osuka, A.; Kim, D. *J. Phys. Chem. B* **2005**, *109*, 11223−11230.

(28) Kasha, M.; Rawls, H. R.; El-Bayoumi, M. A. *Pure Appl. Chem.* **1965**, *11*, 371−392.

(29) Brocklehurst, B.; Young, R. N. *J. Chem. Soc., Faraday Trans.* **1994**, *90*, 2001−2001.

(30) Lin, V. S. Y.; Therien, M. J. *Chem. Eur. J.* **1995**, *1*, 645−651.

(31) Bothner-By, A. A.; Dadok, J.; Johnson, T. E.; Lindsey, J. S. *J. Phys. Chem.* **1996**, *100*, 17551−17557.

(32) Wilson, G. J.; Arnold, D. P. *J. Phys. Chem. A* **2005**, *109*, 6104−6113.

(33) Gouterman, M. *J. Chem. Phys.* **1959**, *30*, 1139−1161.

(34) Gouterman, M. *J. Mol. Spectrosc.* **1961**, *6*, 138−163.

(35) Drobizhev, M.; Stepanenko, Y.; Dzenis, Y.; Karotki, A.; Rebane, A.; Taylor, P. N.; Anderson, H. L. *J. Phys. Chem. B* **2005**, *109*, 7223−7236.

(36) Hindin, E.; Forties, R. A.; Loewe, R. S.; Ambroise, A.; Kirmaier, C.; Bocian, D. F.; Lindsey, J. S.; Holten, D.; Knox, R. S. *J. Phys. Chem. B* **2004**, *108*, 12821−12832.

(37) Frisch, M. J.; Trucks, G. W.; Schlegel, H. B.; Scuseria, G. E.; Robb, M. A.; Cheeseman, J. R.; Montgomery, J. A., Jr.; Vreven, T.; Kudin, K. N.; Burant, J. C.; Millam, J. M.; Iyengar, S. S.; Tomasi, J.; Barone, V.; Mennucci, B.; Cossi, M.; Scalmani, G.; Rega, N.; Petersson, G. A.; Nakatsuji, H.; Hada, M.; Ehara, M.; Toyota, K.; Fukuda, R.; Hasegawa, J.; Ishida, M.; Nakajima, T.; Honda, Y.; Kitao, O.; Nakai, H.; Klene, M.; Li, X.; Knox, J. E.; Hratchian, H. P.; Cross, J. B.; Bakken, V.; Adamo, C.; Jaramillo, J.; Gomperts, R.; Stratmann, R. E.; Yazyev, O.; Austin, A. J.; Cammi, R.; Pomelli, C.; Ochterski, J. W.; Ayala, P. Y.; Morokuma, K.; Voth, G. A.; Salvador, P.; Dannenberg, J. J.; Zakrzewski, V. G.; Dapprich, S.; Daniels, A. D.; Strain, M. C.; Farkas, O.; Malick, D. K.; Rabuck, A. D.; Raghavachari, K.; Foresman, J. B.; Ortiz, J. V.; Cui, Q.; Baboul, A. G.; Clifford, S.; Cioslowski, J.; Stefanov, B. B.; Liu, G.; Liashenko, A.; Piskorz, P.; Komaromi, I.; Martin, R. L.; Fox, D. J.; Keith, T.; Al-Laham, M. A.; Peng, C. Y.; Nanayakkara, A.; Challacombe, M.; Gill, P. M. W.; Johnson, B.; Chen, W.; Wong, M. W.; Gonzalez, C.; Pople, J. A. *Gaussian 03*, revision B.05; Gaussian, Inc.: Pittsburgh PA, 2003.

(38) Becke, A. D. *J. Chem. Phys.* **1993**, *98*, 5648−5652.

(39) Lee, C.; Yang, W.; Parr, R. G. *Phys. Rev. B* **1988**, *37*, 785−789.

(40) Vosko, S. H.; Wilk, L.; Nusair, M. *Can. J. Phys.* **1980**, *58*, 1200−1211.

(41) Ditchfield, R.; Hehre, W. J.; Pople, J. A. *J. Chem. Phys.* **1971**, *54*, 724−728.

(42) Winters, M. U.; Wilson, C. J.; Kärnbratt, J.; Anderson, H. L.; Albinsson, B. *Chem. Eur. J.*, accepted for publication.